Electrospun microstructured PLA-based scaffolds featuring relevant anisotropic, mechanical and degradation characteristics for soft tissue engineering

Louis Gangolphe, Christopher Leon-Valdivieso, Benjamin Nottelet, Stéphane Déjean, Audrey Bethry, Coline Pinese, Frédéric Bossard, Xavier Garric

Version of Record: https://www.sciencedirect.com/science/article/pii/S0928493121004793
Manuscript_2bea7176cfeeda050c00fee2b1c31673

Electrospun microstructured PLA-based scaffolds featuring relevant anisotropic, mechanical and degradation characteristics for soft tissue engineering

Louis Gangolphe[ab], Christopher Y. Leon-Valdivieso[a], Benjamin Nottelet[a], Stéphane Déjean[a], Audrey Bethry[a], Coline Pinese[a], Frédéric Bossard[b*], Xavier Garric[a]*

[a]*Department of Polymers for Health and Biomaterials, Max Mousseron Institute of Biomolecules (IBMM), UMR CNRS 5247, University of Montpellier, France*

[b]*Univ. Grenoble Alpes, CNRS, Grenoble INP*, LRP, 38000 Grenoble, France * Institute of Engineering Univ. Grenoble Alpes*

[*]*corresponding authors:*

xavier.garric@umontpellier.fr

frederic.bossard@univ-grenoble-alpes.fr

Graphical Abstract

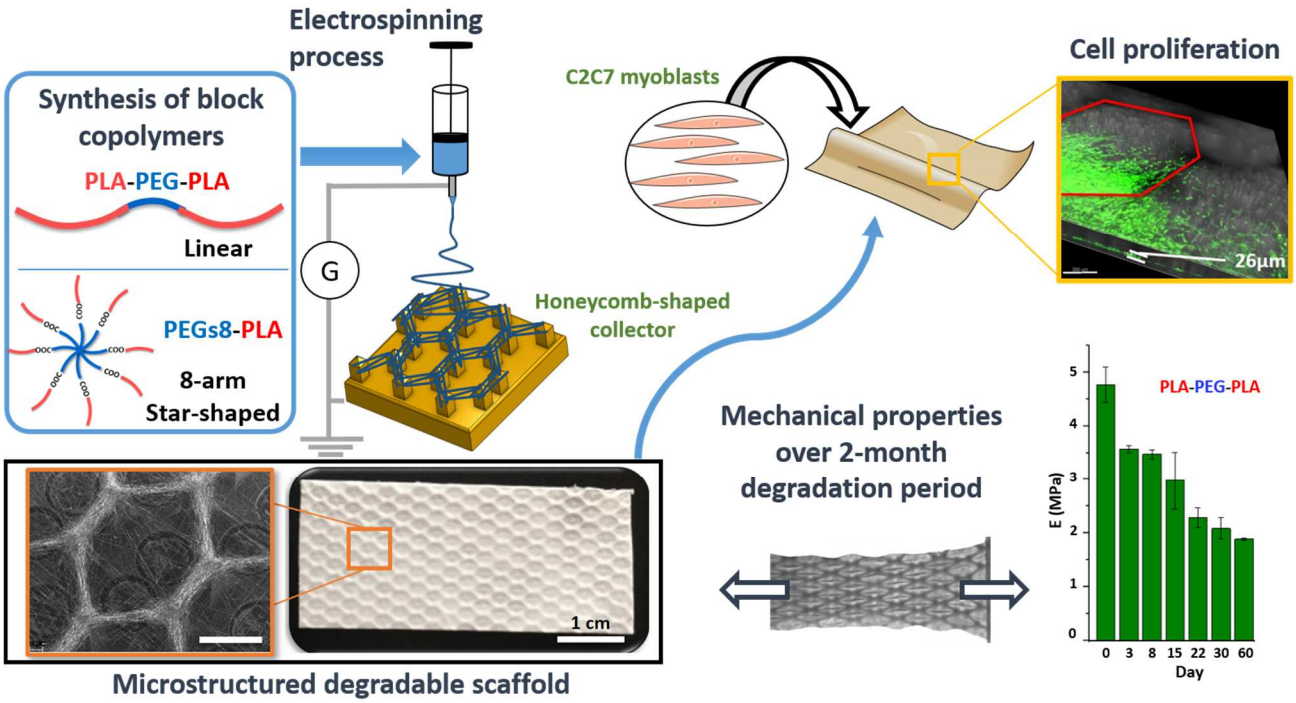

Abstract

Electrospun scaffolds combine suitable structural characteristics that make them strong candidates for their use in tissue engineering. These features can be tailored to optimize other physiologically relevant attributes (e.g. mechanical anisotropy and cellular affinity) while ensuring adequate degradation rates of the biomaterial. Here, we present the fabrication of microstructured scaffolds by using a combination of micropatterned electrospinning collectors (honeycomb- or square-patterned) and poly(lactic acid) (PLA)-based copolymers (linear or star-shaped). The resulting materials showed appropriate macropore size and fiber alignment that were key parameters to enhance their anisotropic properties in protraction. Moreover, their elastic modulus, which was initially similar to that of soft tissues, gradually changed in hydrolytic conditions, matching the degradation profile in a 2- to 3-month period. Finally, honeycomb-structured scaffolds exhibited enhanced cellular proliferation compared to standard electrospun mats, while cell colonization was shown to be guided by the macropore contour. Taking together, these results provide new insight into the rational design of microstructured materials that can mimic the progressive evolution of properties in soft tissue regeneration.

Keywords

Degradable polyester block copolymer

Electrospinning

Microstructured scaffold

Mechanical properties

Cell proliferation

1. Introduction

Damaged native soft tissues are often the cause of major chronic health problems (potentially leading to tissue or organ failure) with an equally important economic impact [1]. Tissue transplantation is the most widespread used method to restore damaged or lost tissues. It presents, nevertheless, several downsides such as shortage of tissue donors, the loss of biological function in the site of tissue extraction and immuno-rejection of the transplanted tissue (particularly when an allograft is employed), which diminishes relevance and applicability of this procedure [1,2]. The increasing trend of tissue engineering alternatives over transplantation is based on the successful development of biomaterials (either from biological or synthetic sources) that recapitulate the biological and physical characteristics of the damaged (or lost) tissue/organ and allow its further *de novo* formation [3]. Among the different strategies to fabricate cellular scaffolds [4], electrospinning stands out as a facile and versatile process to produce nano-to-micron sized polymeric fibrillar mats, resembling the rather complex extracellular matrix (ECM) architecture [5–7]. One of the major drawbacks of this technique is the poor cellular infiltration and migration that electrospun scaffolds exhibit because of their highly packed fibers, thus reducing the advantages of 3D tissue cultures in these materials. To overcome this problem, different research groups have proposed the use of microstructured collectors [8,9] to induce and tailor the formation of macropores that ensure adequate cell penetration and nutrients diffusion. These macropores also impart directionality to the fibers, a structural feature that has proved to promote biological processes such as cellular migration and proliferation [10,11]. Moreover, orientation of fibers can also influence the mechanical anisotropy of the scaffold [7], an attribute that permits engineered tissues to maximize their performance in the preferred direction of function and that is (most of the time) overlooked during scaffold designing [12]. Besides, ideal scaffold candidates must feature mechanical strength similar to that of native tissues while ensuring adequate degradation times that match ECM formation and healing processes, therefore avoiding post-

operation removal [13,14]. Consequently, the choice of a polymer remains crucial to modulate the expected gradual change of mechanical properties/cues which have a significant impact on the cellular behavior at different stages of the regenerative process [14].

To the best of our knowledge, only a few studies have been conducted on electrospun degradable polymers combined with microstructured collectors; the most relevant among them are based on poly(lactic acid) (PLA) [10], poly(lactic-*co*-glycolic acid) (PLGA) [15], PLA/collagen [16] and poly(ε-caprolactone) (PCL) [17,18]. While PCL has shown a greater ease to conserve the macroporous structure over time compared to PLA [19], its hydrolytic degradation proceeds more slowly than PLA or PLGA [20,21]. On the other hand, the use of PLA has been limited so far to the fabrication of thin microstructured scaffolds with thickness lower than 100 µm (hence similar to 2D models), or thicker scaffolds that require longer collection times but exhibit a notable loss of structuration [22,23]. As a matter of fact, increasing the thickness of the polymeric network to several hundreds of microns without losing the macrostructure design remains still a challenge [19,22]. Previous reports from our group have shown the feasibility of synthesizing aliphatic block copolymers based on PLA and poly(ethylene glycol) (PEG): PLA-*b*-PEG-*b*-PLA (linear) and PEG_{8arm}10k-*b*-PLA (star-shaped) [24–26]. These copolymers combine PLA favorable mechanical properties and biocompatibility (being used in FDA-approved applications) with the hydrophilic behavior imparted by the inert PEG moiety, opening the possibility to produce electrospun biomaterials with tailorable (hydrolytic) degradation rate and intrinsic fiber mechanical strength.

Herein, we propose the fabrication of macroporous PLA-based biomaterials by exploiting the versatility of electrospinning method in order to: 1) dictate the fiber orientation to promote the scaffold's mechanical anisotropy, 2) provide sufficient native-tissue-like strength during healing processes while ensuring gradual degradation times and 3) guarantee nutritional diffusion and support cellular proliferation and colonization across the scaffold. To this end, we have synthesized a library of our custom-made block copolymers to explore different characteristics: i) molecular structure – linear (PLA-*b*-PEG10k-*b*-PLA) and star-shaped (PEG_{8arm}10k-*b*-PLA), ii) the degree of crystallinity given by the D-to-L enantiomeric ratio in PLA and iii) the final molecular weight of the copolymer. Selected copolymers were electrospun into different microstructures and the resulting scaffolds were then evaluated in terms of morphology, mechanical properties, degradation and biological behavior. The combination of our tailorable copolymers and appropriate micro-architectures gathers promising features for further development of scaffolds for soft tissue engineering.

2. Materials and Methods

2.1 Materials

D,L-lactide (L/D enantiomeric ratio = 50/50 or 94/6; referred to as 50 and 94, respectively) was purchased from Corbion (Gorinchem, The Netherlands). 8-arm poly(ethylene glycol) (tripentaerythritol core) ($PEG_{8arm}10k$, Mw = 10 000 $g.mol^{-1}$) was purchased from JenKem Technology Co., Ltd (Beijing, China). Poly(ethylene glycol) (PEG10k, Mw = 10 000 $g.mol^{-1}$), tin(II) 2-ethylhexanoate ($Sn(Oct)_2$, 95%), dichloromethane (DCM), diethylether (Et_2O) and N,N-dimethylformamide (DMF) were purchased from Sigma-Aldrich (St Quentin Fallavier, France).

2.2 Synthesis of Copolymers

Triblock copolymers PLA-*b*-PEG10k-*b*-PLA and diblock copolymers $PEG_{8arm}10k$-*b*-PLA were synthesized *via* ring-opening polymerization (ROP) as described in a previous report [27]; final molecular weights of 100 000 and 200 000 $g.mol^{-1}$ were targeted for each copolymer. This procedure is reported in Supplementary information along with the physico-chemical characterization methods (sections SI.1 and SI.2).

PLA-b-PEG10k-b-PLA

^1H NMR (300 MHz; $CDCl_3$): δ (ppm) = 5.1 (q, 1H, CO–C***H***—(CH_3)–O), 3.6 (s, 4H, C***H*****$_2$**—C***H*****$_2$**–O), 1.5 (m, 3H, CO–CH(C***H*****$_3$**)–O). (Figure S1)

$PEG_{8arm}10k$-b-PLA

^1H NMR (300 MHz; $CDCl_3$): δ (ppm) = 5.1 (q, 1H, CO–C***H***—(CH_3)–O), 4.3 (m, 2H, O-CH_2-C-C***H*****$_2$**-O), 3.6 (s, 4H, C***H*****$_2$**—C***H*****$_2$**–O), 3.3 (m, 2H, O-C***H*****$_2$**-C-CH_2-O), 1.5 (t, 3H, CO-CH—(C***H*****$_3$**)-O). (Figure S2).

Please note that for sake of clarity we have adopted a generic nomenclature for the library of all the resulting block copolymers as follows:

PLA-*b*-PEG10k-*b*-PLA -> PLA**x**-PEG-PLA**x***Y*

PEG_{8arm}10k-*b*-PLA -> PEGs8-PLA**x***Y*

where the subindex **X** denotes the PLA L/D ratio (50 or 94) and *Y* the molecular weight of the copolymer (100 or 200 for 100 000 or 200 000 $g.mol^{-1}$, respectively).

2.3 Electrospinning

Selected PLA-PEG-PLA or PEGs8-PLA block copolymers were dissolved in a DCM/DMF mix (70/30 v/v) at concentrations ranging from 9 to 35 wt% (Table S1). The copolymer solution was transferred into a 5 mL syringe attached to a 21-gauge needle; the syringe was loaded onto a vertical syringe holder connected to an automatic KDS Legato 200 syringe pump (KD Scientific, Holliston, MA, USA) and a flow rate of 1.8 $mL.h^{-1}$ was set. The distance from the brass micro-structured collector (square-or –honeycomb shaped, fabricated *via* Electrical Discharge Machining (EDM)) to the tip of the needle was kept at 15 cm, while the collector's temperature was maintained at 28 ± 2°C using a MINICOR 55 temperature regulator. A constant potential difference of 15 kV was applied throughout the whole process with a homebuilt high-voltage electrical generator (Iseg GmbH, Radeberg, Germany). Experiments were performed at 21 ± 1°C with a relative humidity of 43 ± 3%. To fabricate randomly-oriented scaffolds, a (non-heated) flat aluminum foil collector was used while keeping the rest of the electrospinning parameters unchanged. All the produced scaffolds were dried overnight before further characterization.

2.4 Degradation Study

Electrospun scaffolds (15 × 15 mm) were weighed (mi = initial mass), immersed in 6 mL of phosphate buffered saline (PBS, pH = 7.4) and kept at 37°C under constant stirring. At different timepoints, samples were removed from PBS, weighed (mw = mass of the wet samples) and dried to constant mass (mx = dry mass after x time in PBS). The water uptake and remaining mass of the scaffolds were calculated from equations 1 and 2, respectively.

Eq. 1: $Water\ uptake\ (\%) = \frac{mw-mi}{mi} * 100$

Eq. 2: $Remaining\ mass\ (\%) = \left(1 - \frac{mi-mx}{mi}\right) * 100$

The molecular weight and dispersity of dried samples were determined with Size Exclusion Cromatography (SEC). Instrument and method can be found in the supplementary material (section SI.2).

2.5 Tensile tests

The mechanical properties of electrospun scaffolds were measured in elongation with an ARES G2 rotational rheometer (dynamic mechanical testing mode; TA Instruments, United States) equipped with a 20 N normal force sensor (0.001 N precision). Samples (30 × 10 mm)

of known thickness were analyzed in linear tension at room temperature (21 ± 1°C) in their dry state; while for the hydrated state, samples were immersed in deionized water at 37°C for 6 hours using a BioPuls Bath (Instron, United States), prior to the tensile test. A deformation rate of 10 mm.min^{-1} was used for all the experiments. Young's modulus (E, MPa), stress at yield (σ_{yield}, MPa), strain at yield (ε_{yield}, %), stress at break (σ_{break}, MPa) and strain at break (ε_{break},%) were expressed as the mean value of three measurements for each condition. The yield point was determined at 5% offset in the initial slope of the stress-strain curve.

2.6 Cellular Behavior

Cell culture

C2C7 myoblasts (kindly provided by Prof. Mercier's lab, PhyMedExp, University of Montpellier, France) were cultured (either during expansion in plastic or when seeded in the electrospun scaffolds) in DMEM high glucose supplemented with 10% Fetal Bovine Serum (FBS), 2 mM L-glutamine and 1% penicillin/streptomycin and cultured at 37°C and 5% CO_2 under sterile conditions.

NIH3T3/GFP murine cells (Cell Biolabs, batch 72720170-4) were grown in DMEM high glucose supplemented with 5% Fetal Bovine Serum (FBS), 2 mM L-glutamine, 0.1 mM MEM Non-Essential Amino Acids (NEAA), 1% penicillin/streptomycin and 10 µg.mL^{-1} blasticidin, cultured at 37°C and 5% CO_2 under sterile conditions. Both cell lines were tested for mycoplasma contamination and passaged at 80% confluence.

Proliferation assay

Scaffolds were sterilized with UV-C radiation (2-minute exposure on each side) prior to placing them on a 24-well plate (non-treated) and kept them fixed with o-rings. The samples were then soaked for 90 min in ethanol (70% v/v) twice and finally washed with phosphate-buffered saline (PBS) three times. Cell growth medium was added to each well (2 mL) and myoblasts were seeded (final concentration = 5.1x10^5 cells/mL) and allowed to attach to the scaffold at 37°C. After 3 hours, growth medium was exchange for fresh one to remove non-adherent cells.

PrestoBlue® assay (Invitrogen A13262) was used to determine cell viability at 24, 48, 72 and 96 h according to the supplier instructions. Briefly, PrestoBlue® cell viability reagent in a 1:10 volume ratio with growth medium was added to each well and incubated in the dark for 30 min at 37°C. Fluoroscence intensity of the supernatant was measured (wavelength: 558 nm

excitation, 590 nm emission) in a CLARIOstar® microplate reader. After each measurement, fresh medium was used to wash the samples and also added to continue with the culture.

Cell colonization assay

Sterile scaffolds were placed in 23 mm FluoroDish cell culture dishes and positioned in the center with o-rings. Then, a removable culture-insert 2 well (Ibidi) was placed in the midle of the scaffold followed by the addition of growth medium and 6 x 10^4 cells (NIH3T3 GFP cell line) in each well. After 4h at 37°C, both growth medium and culture insert were removed and fresh medium was added in each culture dish, allowing the seeded scaffold to incubate at 37°C up to sixteen days in sterile conditions. Samples were imaged on days 3, 9 and 16 under controlled atmosphere (37°C and 5% CO_2) using a NikonTi2 inverted epifluorescence microscope (10X objective lense) and an Andor Dragonfly® inverted confocal spinning disk (20X and 40X objective lenses).

R software version 3.5.2 was used to perform statistical analysis. Each experimental evaluation was performed in sextuplicate. Significance was assessed by 2-way ANOVA with repeated measures followed by Tukey test (multiple comparisons). Values of *P <0.05 were considered as statistically significant; **P <0.01; ***P <0.001.

3. Results and discussion

The selection of a polymeric biomaterial is generally based on their ability to match physiologically-adequate mechanical properties, degrade consistenly over time and to ensure cytocompatibility and cell adhesion to promote the re-establishment of tissues along with their biological functions [3]. PLA was chosen as a suitable candidate due to its biocompatibility (FDA-approved for medical devices), sufficient mechanical strength and biodegradability [24], while association with PEG offers the possibility to modulate the hydrophilic behavior of the final structured material (thus the mechanical properties and degradation rate). Moreover, copolymerization of PLA with PEG would avoid the well-studied phase separation phenomena and surface erosion on electrospun fibers, arising from the different surface energies (hence limited miscibility) between the two polymers when they are blended [28].

3.1 Synthesis and processing of block copolymers

We have synthesized by ROP in bulk a library of PLA-PEG block copolymers with aim to screen the following design parameters: i) molecular weight (100 000 or 200 000 $g.mol^{-1}$), ii) macromolecular structure (linear or star-shaped) and iii) the degree of crystallinity

(amorphous PLA_{50} or semi-crystalline PLA_{94}). In all the cases, the molecular weight of PEG core (linear or star-shaped) was kept at 10 000 $g.mol^{-1}$ based on the ease of clearance upon degradation of ester bonds contained in PLA moieties (PEG is cleared from the body at molecular weights below 20 000 $g.mol^{-1}$ [29]).

The characterization results of the produced block copolymers are summarized in Table 1. First, while there is a good agreement between the theoretical and experimental molecular weight determined by ^{1}H NMR ($\overline{\boldsymbol{Mn}}_{NMR}$, calculated from the ratio of characteristic PLA (5.1 ppm –CH group) and PEG (3.6 ppm $–CH_2$ group) integration peaks), lower $\overline{Mn}$ values were obtained with SEC for a given copolymer (e.g., PLA_{50}-PEG-PLA_{50}100: $\overline{\boldsymbol{Mn}}_{NMR}$= 104 900 $g.mol^{-1}$ *vs.* $\overline{\boldsymbol{Mn}}_{SEC}$ = 41 000 $g.mol^{-1}$). We ascribed the latter to be the result of the amphiphilic behavior of the synthesized materials, leading to variations in their hydrodynamic volume and thus underestimating the molecular weight in the chromatographic method [30,31]. Moreover, the dispersity of the linear block copolymers varied from 1.6 to 1.8 while the star-shaped version ranged from 1.3 to 1.5; this is a notable indication of a more homogeneous mass distribution when compared to similar materials produced by ROP in solution [32]. Second, the measured thermal properties corroborated important differences between the block copolymers. Interestingly, increasing the final molecular weight (i.e. the lactic acid/ethylene glycol ratio) led to an increase in the glass transition temperature (Tg) regardless the type of macromolecular structure (e.g. PLA_{50}-PEG-PLA_{50}100 Tg = 26°C *vs.* PLA_{50}-PEG-PLA_{50}200 Tg = 43°C). A similar trend was found by introducing a higher degree of crystallinity, particularly, for the star-shaped polymers (e.g. PEGs8-PLA_{50}200 Tg = 36°C *vs.* PEGs8-PLA_{94}200: Tg = 46°C).

Electrospun fibers were collected into square and honeycomb-like shapes by using EDM-made collectors (Figure 1A). These macrostructured templates consist on different millimeter-sized peak arrays where the electric field is preferentially distributed on, improving the electrical point effect and dictating the way fibers are deposited [10]. Fibers are initially attracted and accumulated onto the peaks surface; then, charged fibers would stretch over to interconnect with the nearest conductive peak, leading to the formation of the corresponding sides and vertices of squares or hexagons, with a rather low probability of fibers crossing the central gap of the structure as it represents a longer path for the fiber to fly across [10]. This repeating process allowed the fabrication of patterned scaffolds (Figures 1B and 1C) characterized by distinct high fiber density zones located on peaks and between neighboring peaks, and lower density zones in the center of the elementary patterns, promoting a tunable

anisotropy [33]. Mats with randomly-oriented fiber distribution were also fabricated as standard controls (Figure 2A, bottom panel).

Table 1. Library of copolymers synthesized in this work along with their number average molecular weight ($\overline{Mn}$), dispersity ($Đ$), glass transition temperature (Tg) and melting point (mp). Two types of copolymer were produced: PLA$_{\mathbf{X}}$-PEG-PLA$_{\mathbf{X}}Y$ (linear) and PEGs8-PLA$_{\mathbf{X}}Y$ (star-shaped), with subindex **X** being the PLA L/D ratio (50 or 94 for amorphous or semi-crystalline, respectively) and Y the theoretical molecular weight of the copolymer (*100* or *200* for 100 000 or 200 000 g.mol^{-1}, respectively).

Type of block copolymer	$\overline{Mn}$ **NMR (g.mol^{-1})**	$\overline{Mn}$ **SEC (g.mol^{-1})**	$Đ$	**Tg (°C)**	**mp (°C)**
PLA$_{50}$-PEG-PLA$_{50}$*100*	104 900	41 000	1.8	26	/
PLA$_{50}$-PEG-PLA$_{50}$*200*	197 000	148 000	1.8	43	/
PLA$_{94}$-PEG-PLA$_{94}$*200*	191 000	144 000	1.6	44	148.0
PEGs8-PLA$_{50}$*100*	100 000	64 000	1.3	32	/
PEGs8-PLA$_{50}$*200*	221 000	99 000	1.5	37	/
PEGs8-PLA$_{94}$*200*	212 000	138 000	1.4	46	149.0

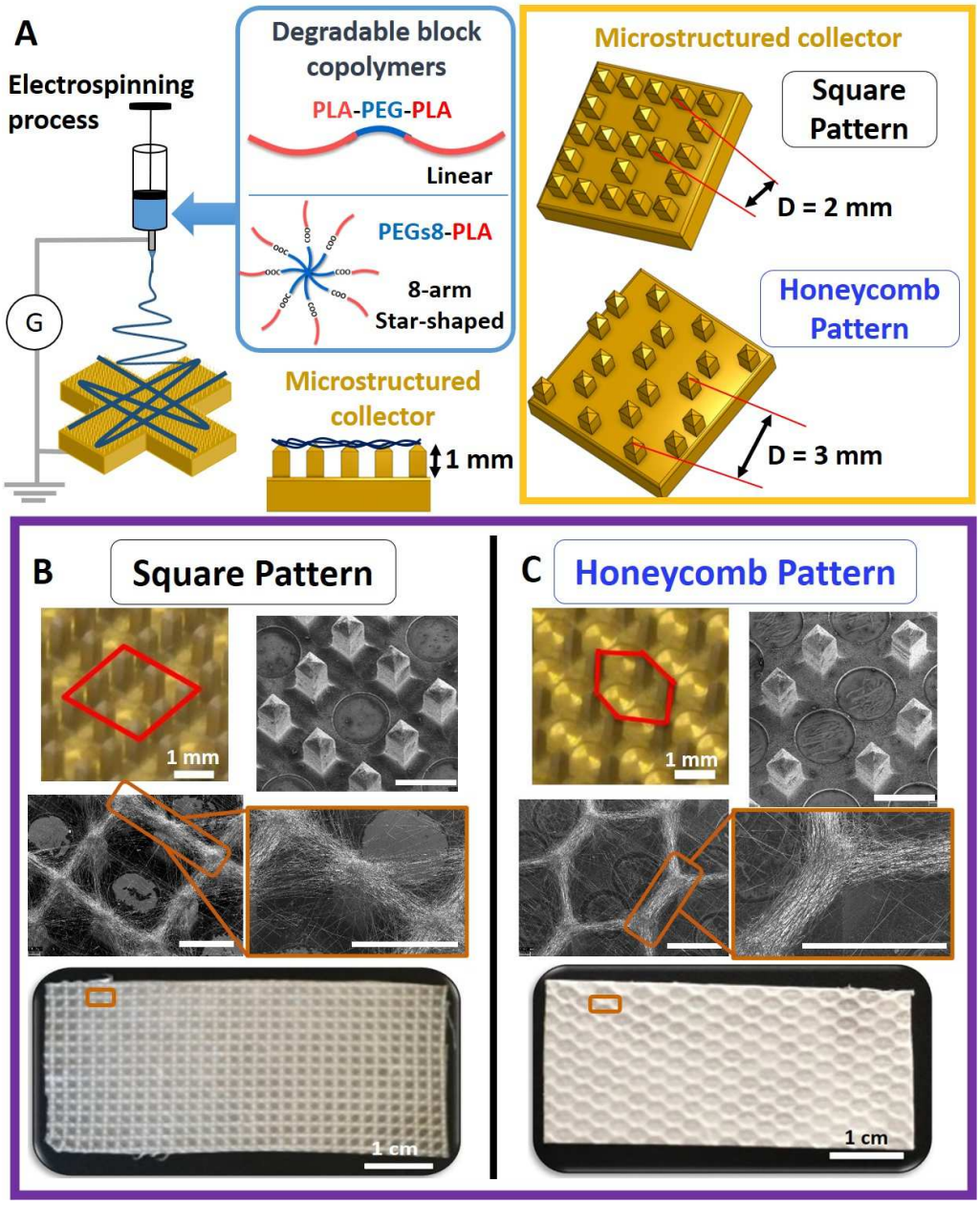

Figure 1: Sample of microstructured scaffolds obtained by electrospinning: (**A**) Electrospinning setup and representation of the two types of patterned collectors used in this work; micrographs of collectors before and after fiber deposition as well as the final electrospun mats for (**B**) square and (**C**) honeycomb patterns.

While we tested the electrospinnability of all the produced block copolymers (Table S1), we also hypothesized that the ones with the lowest Tg (i.e. PLA_{50}-PEG-$PLA_{50}100$, PLA_{50}-PEG-$PLA_{50}200$, PEGs8-$PLA_{50}100$ and PEGs8-$PLA_{50}200$) would facilitate the fabrication of electrospun fibers featuring high degree of orientation in temperature controlled collectors. Indeed, polymers in their rubbery state present high conductivity and a minimized electrostatic shield phenomenon [34], which would be beneficial for the deposition of orderly aligned fibers and to prevent a potential loss of expected architecture in the final scaffold. It

must be noted that copolymers with increased molecular weight (PLA_{50}-PEG-PLA_{50}*200* and PEGs8-PLA_{50}200) exhibited higher intrinsic viscosities (Figure S3) which made some of the solutions rather difficult to electrospin. Moreover, their higher LA/EG ratio also affected the neat structuration of the macropores; for instance, evaluation of PEGs8-PLA_{50}200 electrospun mats showed a very poor (almost non-existent) fiber alignment at 20 minutes of deposition (Figure S4). Conversely, copolymers with lower molecular weight (PLA_{50}-PEG-PLA_{50}100 and PEGs8-PLA_{50}100) were easier to electrospin and did not present any major loss of microstructure during the same deposition time. Based on this, we established a collection time of 20 min that is sufficient to reach a mat thickness of 250 µm which is above than the reported values for similar microstructured materials [22,23], adding relevance to our scaffolds in terms of 3D cellular environment. Therefore, only PLA_{50}-PEG-PLA_{50}100 and PEGs8-PLA_{50}100 were considered as the most promising candidates to produce microstructured scaffolds (from here on referred only as PLA-PEG-PLA and PEGs8-PLA, respectively) and thus further characterization was focused on these two copolymers.

The structural characterization of these scaffolds revealed fiber features that changed according to the template and type of copolymer used. First, directionality of fibers between two interconnected peaks varied according to the collector used (e.g. 0° or -45° for square or honeycomb-like pores, respectively), although unimodal distributions were less evident in square patterns (Figures 2A and 2B); the latter can be attributed to the electrostatic repulsion caused by the accumulation of charged fibers over time [22,35], affecting their orientation to a higher extent when the template peaks are closer to each other (square template area = 4 mm; honeycomb template area = 5.7 mm). Second, the average fiber diameter remained on the microscale for both copolymers (2.60 ± 0.34 µm and 2.66 ± 0.32 µm for PLA-PEG-PLA and PEGs8-PLA, respectively) and even if inter-peak fibers experienced a certain degree of elongation (hence thinning), their diameter did not present any substantial change compared to those located on top of individual peaks (Figure 2C). Different reports have shown that micron-scale fibers present a highly interconnected pore area which facilitates cellular infiltration and diffusion of nutrients, resulting in higher proliferation/infiltration of endothelial cells and fibroblasts when compared to nanofibers [36,37]. Thirdly, the heterogeneous collection of fibers dictated by the peaks rendered a higher porosity in microstructured scaffolds compared to flat collectors (Figure 2D). This significant decrease in fiber density (provoked by the formation of macropores [38]) was obtained for both copolymers (e.g. PLA-PEG-PLA: 82 ± 1% (square) *vs.* 76 ± 1% (random); PEGs8-PLA: 84%

± 1% (square) *vs.* 71± 2% (random)) while no variation was found between both types of pattern (Table S2). These values are within the range of reported porosities that are required for different cellular activities [39].

Contact angle assays (Figure 2E) showed the hydrophobic character of all the fibrillar scaffolds (>120°); the insertion of hydrophilic groups in the polymer backbone did not affect the hydrophobic behavior of the final material. In other reports, electrospun PLA/PEG blends have also shown a hydrophobic surface which was ascribed to be the result of both methyl group enrichment and fibrillar surface roughness [40]. Moreover, the same authors only found a moderate decrease in hydrophobicity when the PEG content was above 10 wt%; this concentration is, however, ten times higher than in our block copolymers in terms of EG/LA molar ratio. Although it has been generally accepted that hydrophilic surfaces enhance cell adhesion and (overall) biological performance [41], cell-material interactions are rather complex phenomena and therefore water contact angle alone cannot be used as a determinant predictor of cellular attachment [42]. Finally, no significant difference in wettability was spotted between the two types of fabricated microstructure (Table S2).

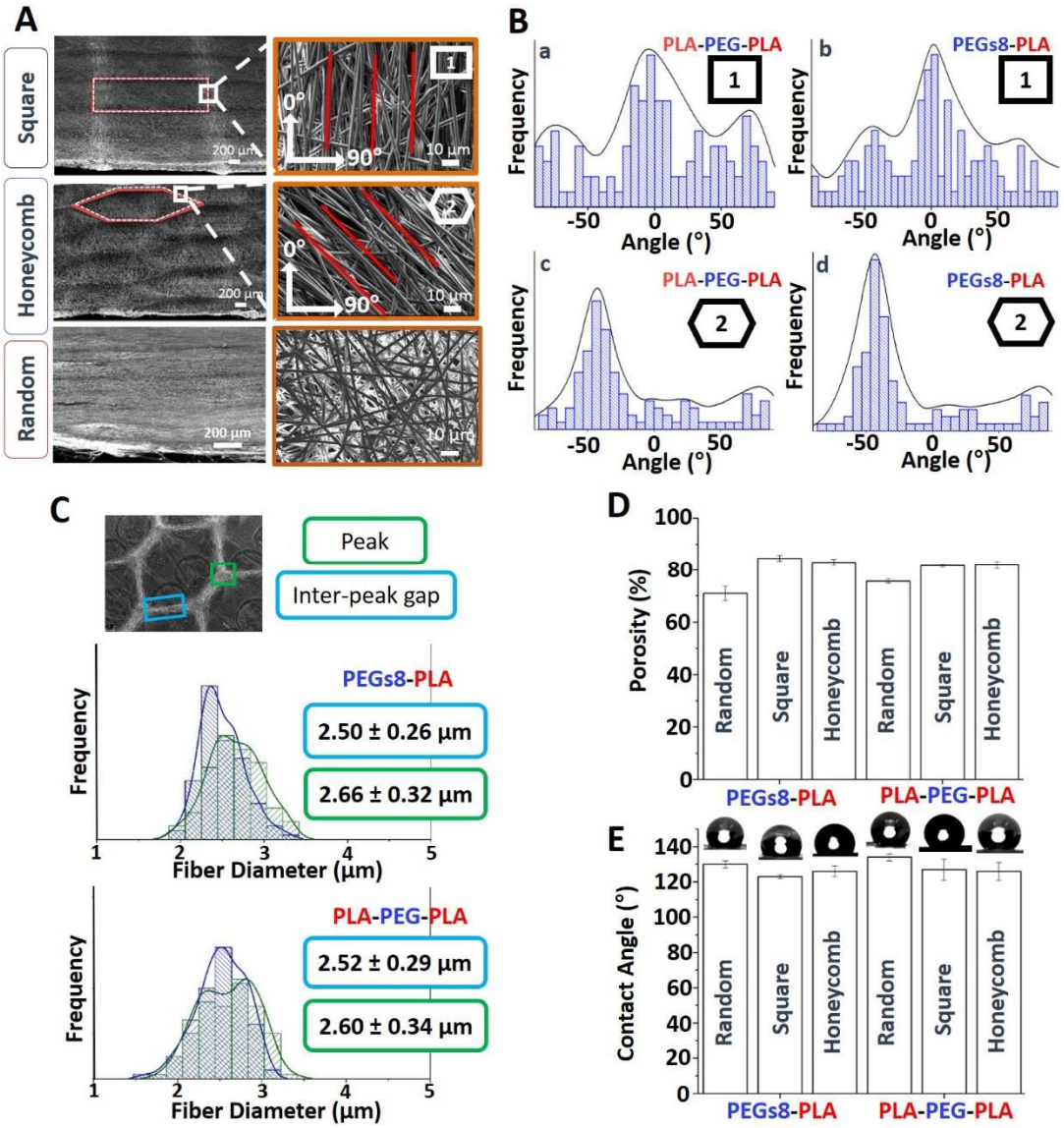

Figure 2. Structural characterization of scaffolds: (**A**) SEM micrographs of patterned (square and honeycomb) and randomly-aligned scaffolds showing the corresponding fiber alignment. (**B**) Dispersity of fiber orientation for square (**a**,**b**) and honeycomb (**c**,**d**) patterns prepared with either PEGs8-PLA or PLA-PEG-PLA. (**C**) Distribution of fiber diameter according to the collection site that allowed the formation of the macropore (peaks, inter-peak gap). Porosity (**D**) and contact angle (**E**) for the different fabricated mats and for both types of copolymer used. Images in **A** were taken from tilted angles to have a view of the topographic relief in both microstructured samples.

3.2 Mechanical properties and anisotropy

Due to the relevance of anisotropy in cellular processes such as attachment and metabolic activity [7,12], we evaluated the mechanical properties of electrospun scaffolds on different tensile orientations (longitudinal and transversal; Figure 3A). Particularly, we were interested in the honeycomb pattern because it exhibited a higher degree of alignment compared to square shape (Figure 2B); results related to the square microstructure can be found in the supplementary information (Figure S5 and Table S3). The anisotropic behavior in the

honeycomb scaffold was evidenced in the strain-stress curves and particularly within the 1-10% deformation range (Figure 3B). The longitudinal elongation rearranged the inter-peak fibers along the tensile direction, inducing a reduction of stress resistance in the low deformation region. On the other hand, the transversal tension prevented the alignment of fibers located perpendicular to the *y* axis in domains of high fiber density (i.e. the pore's contour), generating a higher stress resistance (higher σ_{yield}) compared to longitudinal protraction. We found this phenomenon to be similar for both copolymers. Notably, the patterned scaffolds withstood more deformation without breaking (ε_{break}) than random controls. Specifically, PEGs8-PLA presented a higher tensile strain at break compared to PLA-PEG-PLA, which was accentuated with the longitudinal strecthing ($\varepsilon_{breakPEGs8\text{-}PLA}$= 137±1% (transversal) *vs.* 184±8% (longitudinal); $\varepsilon_{breakPLA\text{-}PEG\text{-}PLA}$= 102±3% (transversal) *vs.* 98±3% (longitudinal)). We believe that these marked anisotropic features in PEGs8-PLA samples are likely to arise from 1) a better distribution of fibers in the macropores (and not in the center) compared to PLA-PEG-PLA (data not shown) and 2) their superior degree of fiber aligment compared to the linear version (Figure 2B, panels c and d).

As seen in Table 2, the final elastic modulus (E) of all the scaffolds remained unchanged regardless the tensile orientation and even the type of copolymer used. A decreased bulk fiber density (caused by the presence of macropores) could play a more important role in the scaffold's strength rather than the fiber re-organization itself, as evidenced by the higher E values for the random version (e.g. $E_{PLA\text{-}PEG\text{-}PLA}$: 41.2 ± 3.2 MPa and 38.7 ± 5.7 MPa for honeycomb, longitudinal and transversal, respectively, *vs.* 90.8 ± 8.4 MPa for random). This trend is in agreement with other reports on 3D composite constructs with hexagonal-shaped pores even with a lower size than ours (D = 160 µm [22]). It is important to note, however, that the porosity of the microstructured scaffolds was not taken into account for the calculation of E, and therefore our results might be underestimated to a certain extent [43].

Table 2: Mechanical properties of (PLA-PEG-PLA or PEGs8-PLA) honeycomb and random scaffolds based on tensile orientation (Longitudinal (Long) or Transversal (Trans)) in dry state at room temperature. *(Data are expressed as means ± SD and correspond to measurements with n=3).*

Copolymer	Scaffold pattern-tensile orientation	σ_{yield} (MPa)	ε_{yield} (%)	σ_{break} (MPa)	ε_{break} (%)	E (MPa)
PLA-PEG-PLA	Honeycomb Long	0.88 ± 0.08	2.6 ± 0.1	1.32 ± 0.12	98 ± 3	41.2 ± 3.2

	Honeycomb Trans	1.07 ± 0.11	3.1 ± 0.1	1.43 ± 0.02	102 ± 3	38.7 ± 5.6
	Random	1.73 ± 0.11	2.0 ± 0.1	2.29 ± 0.07	84 ± 2	90.8 ± 8.4
PEGs8-PLA	Honeycomb Long	0.78 ± 0.14	2.4 ± 0.1	1.36 ± 0.16	184 ± 8	37.2 ± 3.2
	Honeycomb Trans	1.05 ± 0.09	2.6 ± 0.1	1.22 ± 0.12	137 ± 1	35.8 ± 3.5
	Random	2.23 ± 0.08	3.5 ± 0.1	2.44 ± 0.05	99 ± 2	66.8 ± 2.6

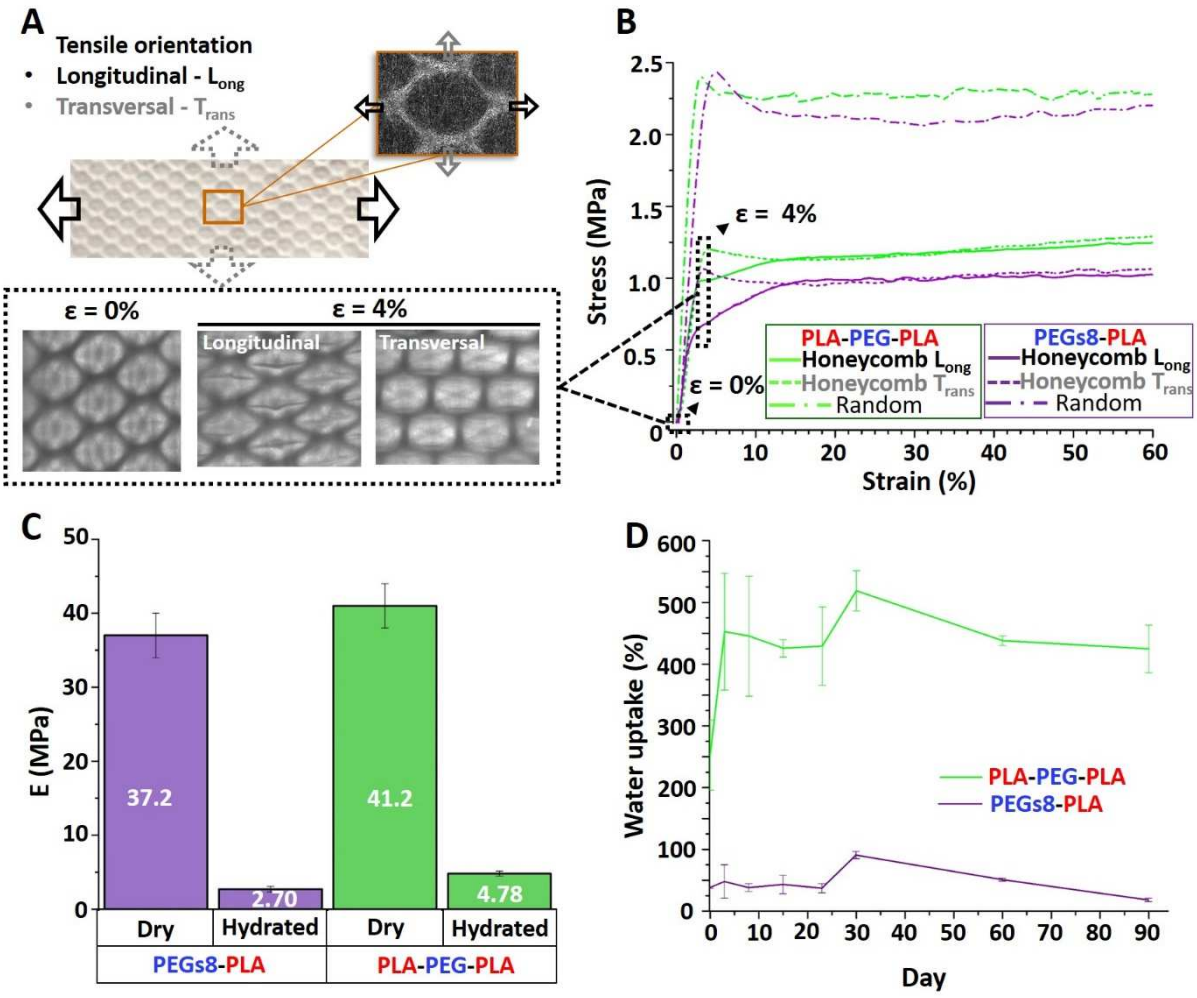

Figure 3: Mechanical properties of microstructured scaffolds: (**A**) top: representation of different tensile orientations in a honeycomb scaffold; bottom: micrographs of unstrained (ε=0%) and elongated (ε=4%) scaffolds. (**B**) Typical stress-strain curves for the honeycomb and random scaffolds made of different copolymers under longitudinal and transversal deformation (dry state at room temperature). (**C**) Young's modulus of the different honeycomb scaffolds in 1) dry state at room temperature and 2) hydrated state at 37°C. (**D**) Water uptake of the different copolymer-based honeycomb scaffolds. *(Data are expressed as means ± SD and correspond to measurements with n=3).*

When elongated (longitudinal tension) in wet conditions at 37°C, the patterned scaffolds showed an almost 10-fold decrease in E (Figure 3C) compared to the dry state (e.g. $E_{PLA\text{-}PEG\text{-}PLA}$: 41.2 ± 3.2 MPa *vs.* 4.78 ± 0.33 MPa for dry and hydrated states, respectively). These results correlate with the water absorption capacity of both copolymers due to PEG's hydrophilicity (interaction with water increases the softness of materials due to plasticization) and the higher molecular chain mobility resulting from raising the temperature above their Tg. Interestingly, the hydrated PEGs8-PLA scaffold exhibited a significantly lower E value (2.70 ± 0.38 MPa) than PLA-PEG-PLA (4.78 ± 0.33 MPa), in spite of presenting a greatly reduced water uptake (Figure 3D). This lower absorption by PEGs8-PLA probably arises from 1) a higher packing density: being protected by eight hydrophobic PLA chains, the PEG core is less accessible to water molecules [44] and 2) a higher degree of chain entanglements, which restrict the mobility of the star-shaped copolymers [29]. Therefore, exposure of PEG moieties to water is not sufficient to explain the difference in mechanical behavior between the two copolymers; other features (e.g. fiber re-arrangement in wet conditions) might have thus a bigger contribution on the elastic strength of these scaffolds. Further, it is worth noting that the resulting Young's moduli from both type of scaffolds are in the order of those commonly found in soft tissues [45].

We next investigated the materials degradation and its effect on the preservation of the mechanical properties, which is one of the major challenges when mimicking healing processes from a tissue engineering perspective [46]. Because of the relevant information gathered on the alignment and mechanical anisotropy of honeycomb scaffolds, we decided to continue further characterization only with this type of microstructure.

3.3 Mechanical properties over degradation time

We evaluated the scaffolds hydrolytic degradation over 90 days with a special focus on the molecular weight, polydispersity and remaining mass, while also tracking the change in mechanical properties in the same timeframe (Figure 4). We found an almost linear decrease of molecular weight for both copolymers, which correlated with the increase in dispersity (Figure 4A); both effects were more pronounced for the star-branched polymer than for the linear version (remaining molecular weight after 90 days: 30% *vs.* 25% and $Đ_{D90}$: 2.3 *vs.* 2.8 for PLA-PEG-PLA and PEGs8-PLA respectively). This difference in degradation can be attributed to the preferential chain scission at the ester linkage between PLA and PEG [28,47] which, above all, occurs differently according to the molecular nature of both copolymers. PLA-PEG-PLA contains two ester groups (one for each PEG-PLA junction) which, after

hydrolysis, would render 2 PLA chain blocks (ideally with a $\overline{Mn}$ = 47 000 g.mol^{-1} from the initial PLA-PEG-PLA with $\overline{Mn}$ = 104 000 g.mol^{-1}) and the original PEG core ($\overline{Mn}$ = 10 000 g.mol^{-1}); whereas PEGs8-PLA possesses eight ester units that, after chain scission, would lead to PLA portions with lower molecular weight and a higher size variability compared to PLA-PEG-PLA. Furthermore, the average mass remained above 90% for both copolymers throughout the whole experiment and the macropore structure was also preserved (Figure 4B). Hydrolytic degradation of PLA blocks progressively generates shorter polymer chains until the formation of water-soluble oligomers ($\overline{Mw} \approx$ 648 g.mol^{-1}) [48]; we believe that cleavage of PLA contained in our scaffolds results in chains that are still large enough to be insoluble in water and to diffuse out of the macrostructure [49], a behavior that is related to its fibrillar nature rather than the geometry itself (Figure S6).

Next, we monitored the evolution of mechanical properties over time of the produced scaffolds (Figure 4C, table S4). It is desirable that such features are maintained during the early stages of regenerative processes, with a moderate but continuous decline that matches the degradation profile and the formation of new ECM [14]. PEGs8-PLA scaffolds exhibited an increase in E after 8 days (2.70 ± 0.38 MPa *vs*. 4.71 ± 0.41 MPa for days 0 and 8 respectively) followed by a drastic drop at day 15 (1.41 ± 0.50 MPa). As no significant difference in molecular weight was observed in the first 8 days, the initial increase of E might be the result of a microphase separation phenomenon caused by the re-arrangement of the PEG core [50,51] during water uptake. Indeed, this would result in regions that are rich in one polymer or another due to a loss of plasticizing effect of PEG and therefore they present an overall increase in stiffness [52]; the subsequent decrease in E can then be attributed to the hydrolytic degradation effects reached from day 15 onwards. After 30 days the low copolymer chain entanglement of PEGs8-PLA honeycomb scaffolds no longer ensured mechanical resistance in our tensile conditions and thus the material became too brittle to be assessed. On the other hand, PLA-PEG-PLA mats showed a reduction of E that remained constant after one week (3.57 ± 0.07 MPa and 3.52 ± 0.09 MPa for days 3 and 8), correlating with the high degree of water uptake (~450%) on the first eight days; this water absorption would lead to a high plasticization effect that may have overshadowed potential microphase separation phenomena, as in the case with PEGs8-PLA, hence the gradual decrease in E from day 0. After 60 days, 40% of the initial elastic modulus remained in the scaffold fabricated with the linear copolymer (E_{D0} = 4.78 ± 0.33 MPa *vs.* E_{D60} = 1.90 ± 0.02 MPa).

Finally, both types of honeycomb scaffolds showed a decrease of σ_{break} over time as expected (Figure 4D). Moreover, ε_{break} drastically decreased after 22 days before exhibiting brittleness. Based previous results of our group, we attributed this phenomenon to the block copolymer's chain scission inducing mechanical changes in the scaffold, switching its behavior from ductile to brittle [25].

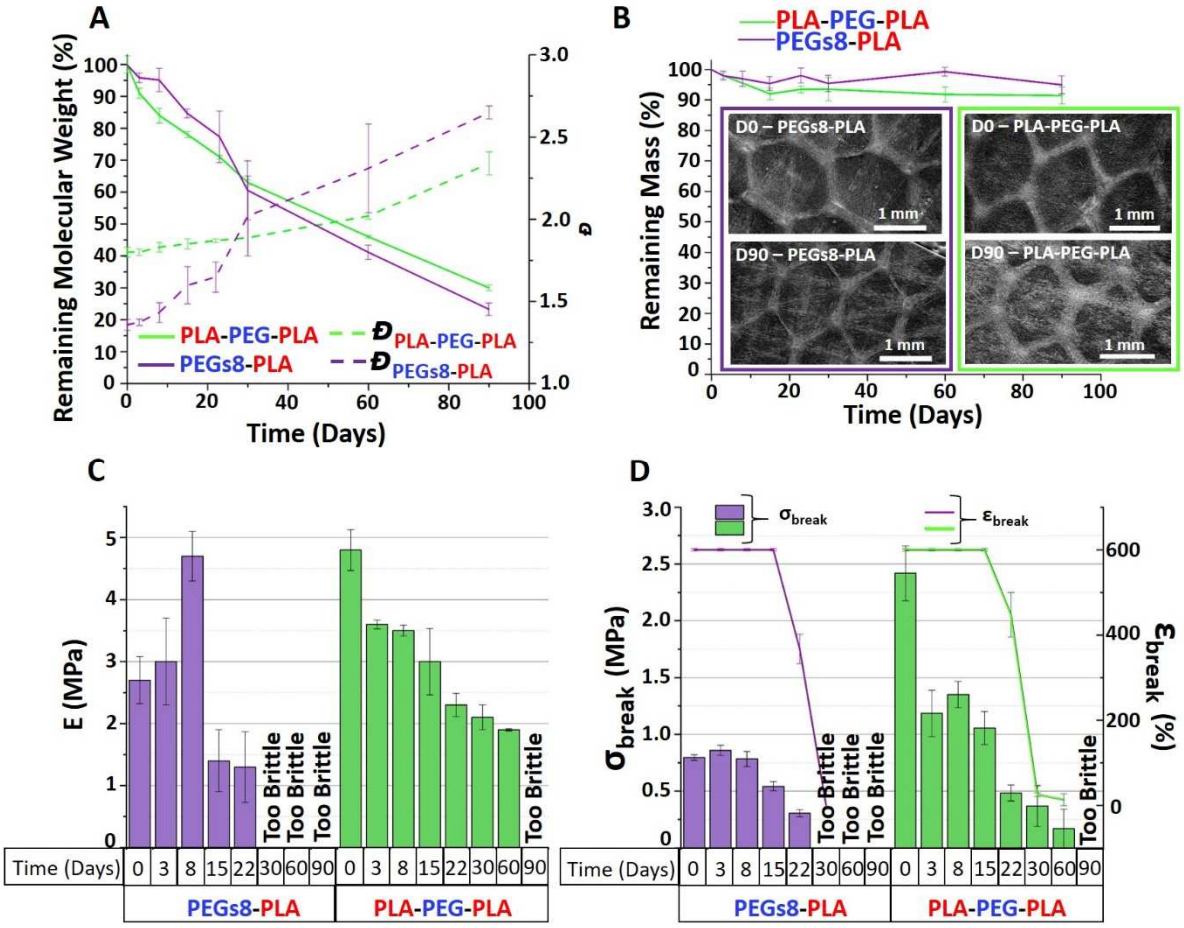

Figure 4. Microstructured scaffolds degradation: (**A**) Remaining molecular weight (%, solid line) and dispersity (dashed line), (**B**) remaining mass (%), (**C**) Young's modulus (E, MPa) evolution and the corresponding (**D**) σ_{break} and ε_{break} of honeycomb scaffolds based on PLA-PEG-PLA and PEGs8-PLA at different timepoints of the hydrolytic degradation assay. Representative SEM images of such samples at D0 and D90 are presented in **B**. *(Data are expressed as means ± SD and correspond to measurements with n=3).*

Considering the results presented in Figure 4, we decided to continue the biological characterization only with PLA-PEG-PLA-based scaffolds for being more relevant at longer times (and thus for healing processes) than PEGs8-PLA which showed brittleness just after 22 days of degradation.

3.4 Cellular proliferation/colonization

The applicability of our microstructured materials for soft tissue regeneration was assessed with the use of myoblasts and (GFP-labelled) fibroblasts. Honeycomb scaffolds prepared with PLA-PEG-PLA started to show a significant enhancement of myoblasts proliferation at 48 h of culture and reached a threefold increase after 96 h compared to the randomly-aligned control (Figure 5A). This improved performance has been corroborated in other reports using a similar honeycomb-like configuration for the proliferation of fibroblasts [53] and embryonic murine C3H10T1/2 cells [17]. Some other authors, however, have found contrasting data. For example, Nedjari *et al.* [54] showed no significant difference in proliferation between their honeycomb and random scaffolds after 6 days when using adipose stem cells. From visual analysis of their scaffolds, we believe their set-up (including the polymer of choice (poly($_L$-lactide-*co*-ε-caprolactone)) did not provide sufficient fiber organization to enhance cell growth, which might have been partially impeded by the selected honeycomb pore size (160 μm).

Fibroblasts, which are the main cells in connective tissue, were used to evaluate the migration in PLA-PEG-PLA scaffolds. They progressively colonized most of the surface area after 16 days of culture (Figure 5B) while ingrowth was also found on the Z axis (depth of the scaffold; Figure 5C, top panels). The latter is likely to be promoted by a combination of two factors: firstly, the milimeter-sized macropores, which are known to facilitate cell migration to different depth levels in electrospun scaffolds compared to micrometric ones [38,55]; and second, the macroscopic interconnectivity provided by the heterogenous distribution of fibers in the macropores (more on the edges and less in the center), enhancing the overall cellular infiltration [38]. Indeed, this distinct fiber density in designated regions of the macropore led to the formation of inter-fiber pores that were larger in central areas compared to the contour (Figure S7), facilitating thus the cellular invasion on the Z direction. Notably, the average pore size of both macropore regions remained within the range that is required for cell-cell communication and migration throughout the scaffold [56]. Furthermore, fibroblasts also appeared to migrate along the honeycomb perimeter (Figure 5C, bottom panels), thus guiding the cell colonization according to the shape of the macropore, which in turn might lead to the possibility of ECM depositon in an organized fashion as reported by other authors [12]. Taking altogether, design parameters of honeycomb scaffolds (such as pore size and fiber density) are key features that can facilitate cell penetration, nutrients diffusion and, ultimately, drive the formation of new soft tissue with anisotropic behavior. Finally, it is important to

mention that our scaffolds experienced a certain degree of shrinkage (≈ 25%), which is a common phenomenon mostly caused by the interaction of the polymeric fibers with the cell culture medium [57].

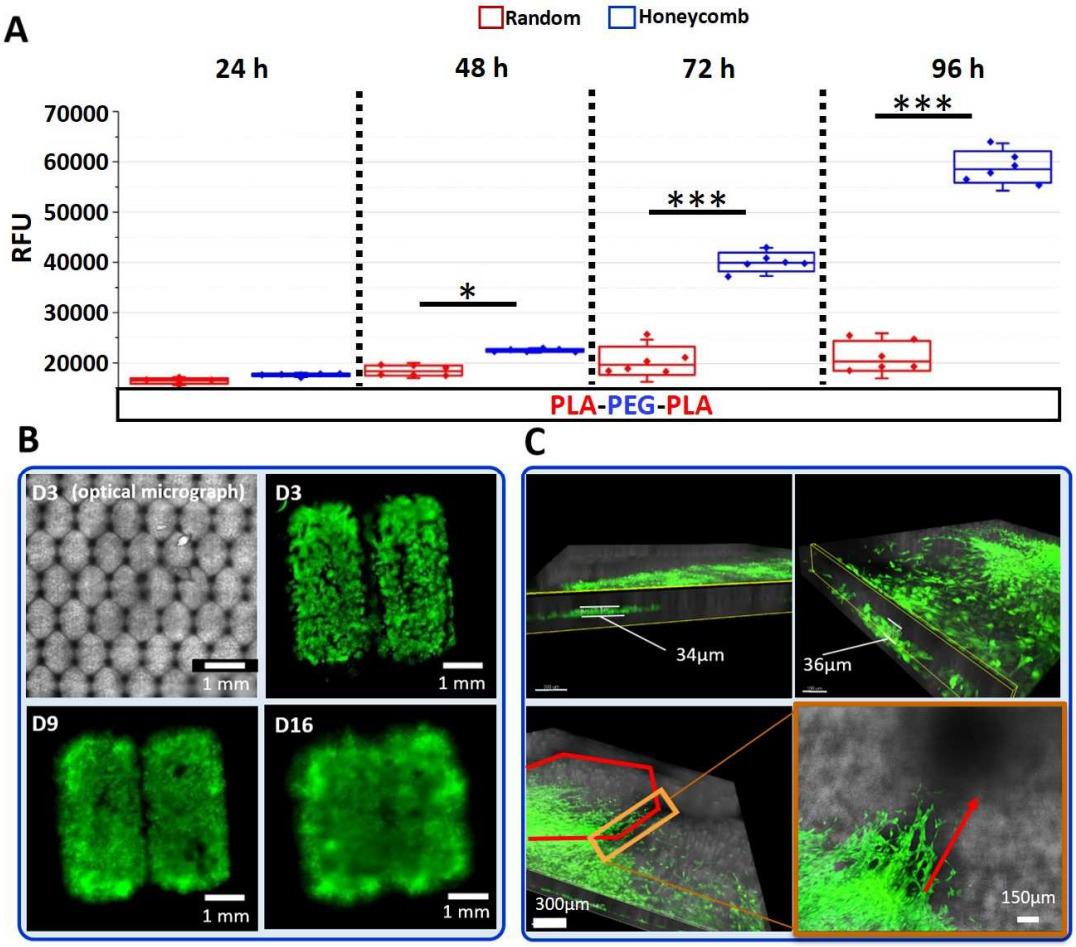

Figure 5: Cell proliferation and colonization on PLA-PEG-PLA microstructured scaffolds: (**A**) C2C7 cell proliferation on honeycomb and random scaffolds at 24h, 48h, 72h and 96h. (**B**) NIH3T3 GFP cell colonization on honeycomb scaffolds made of PLA-PEG-PLA at days 3, 9 and 16; top left micrograph was acquired using bright field mode. (**C**) 3D view of NIH3T3 GFP cell invasion on the same scaffolds after 16 days. *(Each experimental evaluation was performed in sextuplicate. Significance was assessed by 2-way ANOVA with repeated measures followed by Tukey test (multiple comparisons). Values of *P <0.05 were considered as statistically significant; ***P <0.001).*

4. Conclusions

In this work we report the fabrication of microstructured PLA-based electrospun scaffolds that present elastic anisotropy and that are able to maintain the mechanical properties over time in a degradation-induced environment. We particularly investigated honeycomb-patterned scaffolds for presenting a superior fiber alignment compared to the square-patterned type. The resulting orientation of fibers accounted for the anisotropic behavior under tensile

stress for both types of copolymers, with PEGs8-PLA being able to withstand more deformation at break than the linear version PLA-PEG-PLA. Moreover, these scaffolds preserved their macrostructure after 3 months while their initial elastic modulus decreased in a moderate fashion (matching the molecular degradation in hydrolytic conditions), albeit exhibiting comparable values with soft tissues up to 2 months (when PLA-PEG-PLA was used). Additionally, the honeycomb macrostructure showed to improve cellular proliferation compared to non-macroporous randomly-aligned fibers and also to stimulate 3D cellular invasion, which are critical parameters towards the regeneration of tissue. In perspective, further work might consider crosslinking of the polymeric scaffold to retain its physical properties for longer periods as well as tailoring the pore dimension (thus the corresponding fiber density) to engineer homogeneous cellular colonization and anisotropic responses to support the formation and alignment of newly developed ECM.

Acknowledgments

This work was supported by ANR2016-BIOSCAFF (ANR-16-CE09-0024) held by the University of Grenoble-Alpes and the University of Montpellier. The authors wish to acknowledge the support from the Consortium des Moyens Technologiques Communs of Grenoble INP, the Chemistry Platform of IEM Laboratory of the Balard Chemistry pole in Montpellier, on which SEM observations and analyses have been performed, the Synbio3 platform, supported by GIS IBISA and ITMO Cancer, for polymer characterizations and the StatABio platform, BioCampus Montpellier for statistical analysis. ‘‘Laboratoire Rhéologie et Procédés’’ (LRP UMR 5520) is a part of the LabEx Tec 21 (Investissements d'Avenir – grant agreement n° ANR-11-LABX-0030) and participates in the Institut Carnot PolyNat. The Department of Polymers for Health and Biomaterials (Max Mousseron Institute of Biomolecules) participates in the Institut Carnot Chimie Balard Cirimat.

Supplementary information

Supplementary data related to this article can be found online.

Data availability

The raw/processed data required to reproduce these findings are available upon request from the authors.

References

[1] Y. Ikada, Challenges in tissue engineering, J. R. Soc. Interface. 3 (2006) 589–601. https://doi.org/10.1098/rsif.2006.0124.

[2] P.K. Chandra, S. Soker, A. Atala, Chapter 1 - Tissue engineering: current status and future perspectives, in: R. Lanza, R. Langer, J.P. Vacanti, A. Atala (Eds.), Princ. Tissue Eng. Fifth Ed., Academic Press, 2020: pp. 1–35. https://doi.org/10.1016/B978-0-12-818422-6.00004-6.

[3] B.D. Ulery, L.S. Nair, C.T. Laurencin, Biomedical applications of biodegradable polymers, J. Polym. Sci. Part B Polym. Phys. 49 (2011) 832–864. https://doi.org/10.1002/polb.22259.

[4] P. Zhao, H. Gu, H. Mi, C. Rao, J. Fu, L. Turng, Fabrication of scaffolds in tissue engineering: A review, Front. Mech. Eng. 13 (2018) 107–119. https://doi.org/10.1007/s11465-018-0496-8.

[5] N. Masoumi, D. Copper, P. Chen, A. Cubberley, K. Guo, R.-Z. Lin, B. Ahmed, D. Martin, E. Aikawa, J. Melero-Martin, J. Mayer, Elastomeric Fibrous Hybrid Scaffold Supports In Vitro and In Vivo Tissue Formation, Adv. Funct. Mater. 27 (2017) 1606614. https://doi.org/10.1002/adfm.201606614.

[6] L. Min, H. Pan, S. Chen, C. Wang, N. Wang, J. Zhang, Y. Cao, X. Chen, X. Hou, Recent progress in bio-inspired electrospun materials, Compos. Commun. 11 (2019) 12–20. https://doi.org/10.1016/j.coco.2018.10.010.

[7] B. Sun, X.-J. Jiang, S. Zhang, J.-C. Zhang, Y.-F. Li, Q.-Z. You, Y.-Z. Long, Electrospun anisotropic architectures and porous structures for tissue engineering, J. Mater. Chem. B. 3 (2015) 5389–5410. https://doi.org/10.1039/C5TB00472A.

[8] B. Sun, Y.Z. Long, H.D. Zhang, M.M. Li, J.L. Duvail, X.Y. Jiang, H.L. Yin, Advances in three-dimensional nanofibrous macrostructures via electrospinning, Prog. Polym. Sci. 39 (2014) 862–890. https://doi.org/10.1016/j.progpolymsci.2013.06.002.

[9] Y. Zhou, G.Z. Tan, Fabrication of nanofiber mats with microstructure gradient by cone electrospinning, Nanomater. Nanotechnol. 7 (2017) 184798041774847. https://doi.org/10.1177/1847980417748478.

[10] K. Zhang, X. Wang, D. Jing, Y. Yang, M. Zhu, Bionic electrospun ultrafine fibrous poly(L-lactic acid) scaffolds with a multi-scale structure, Biomed. Mater. 4 (2009) 035004. https://doi.org/10.1088/1748-6041/4/3/035004.

[11] A.S. Piotrowski-Daspit, B.A. Nerger, A.E. Wolf, S. Sundaresan, C.M. Nelson, Dynamics of Tissue-Induced Alignment of Fibrous Extracellular Matrix, Biophys. J. 113 (2017) 702–713. https://doi.org/10.1016/j.bpj.2017.06.046.

[12] P. Datta, V. Vyas, S. Dhara, A.R. Chowdhury, A. Barui, Anisotropy Properties of Tissues: A Basis for Fabrication of Biomimetic Anisotropic Scaffolds for Tissue Engineering, J. Bionic Eng. 16 (2019) 842–868. https://doi.org/10.1007/s42235-019-0101-9.

[13] C. Pinese, A. Leroy, B. Nottelet, C. Gagnieu, J. Coudane, X. Garric, Rolled knitted scaffolds based on PLA-pluronic copolymers for anterior cruciate ligament reinforcement: A step by step conception: ROLLED KNITTED SCAFFOLDS, J. Biomed. Mater. Res. B Appl. Biomater. 105 (2017) 735–743. https://doi.org/10.1002/jbm.b.33604.

[14] Q. Chen, S. Liang, G.A. Thouas, Elastomeric biomaterials for tissue engineering, Prog. Polym. Sci. 38 (2013) 584–671. https://doi.org/10.1016/j.progpolymsci.2012.05.003.

[15] S. Zhao, Q. Zhou, Y.-Z. Long, G.-H. Sun, Y. Zhang, Nanofibrous patterns by direct electrospinning of nanofibers onto topographically structured non-conductive substrates, Nanoscale. 5 (2013) 4993. https://doi.org/10.1039/c3nr00676j.

[16] H. Xu, F. Lv, Y. Zhang, Z. Yi, Q. Ke, C. Wu, M. Liu, J. Chang, Hierarchically micro-patterned nanofibrous scaffolds with a nanosized bio-glass surface for accelerating wound healing, Nanoscale. 7 (2015) 18446–18452. https://doi.org/10.1039/C5NR04802H.

[17] A. Garcia Garcia, A. Hébraud, J.-L. Duval, C.R. Wittmer, L. Gaut, D. Duprez, C. Egles, F. Bedoui, G. Schlatter, C. Legallais, Poly(ε-caprolactone)/Hydroxyapatite 3D Honeycomb Scaffolds for a Cellular Microenvironment Adapted to Maxillofacial Bone Reconstruction, ACS Biomater. Sci. Eng. 4 (2018) 3317–3326. https://doi.org/10.1021/acsbiomaterials.8b00521.

[18] N. Lavielle, A. Hébraud, C. Mendoza-Palomares, A. Ferrand, N. Benkirane-Jessel, G. Schlatter, Structuring and Molding of Electrospun Nanofibers: Effect of Electrical and Topographical Local Properties of Micro-Patterned Collectors, Macromol. Mater. Eng. 297 (2012) 958–968. https://doi.org/10.1002/mame.201100327.

[19] S. Nedjari, G. Schlatter, A. Hébraud, Thick electrospun honeycomb scaffolds with controlled pore size, Mater. Lett. 142 (2015) 180–183. https://doi.org/10.1016/j.matlet.2014.11.118.

[20] A. Leroux, T. Ngoc Nguyen, A. Rangel, I. Cacciapuoti, D. Duprez, D.G. Castner, V. Migonney, Long-term hydrolytic degradation study of polycaprolactone films and fibers grafted with poly(sodium styrene sulfonate): Mechanism study and cell response, Biointerphases. 15 (2020) 061006. https://doi.org/10.1116/6.0000429.

[21] A.H. Shamsah, S.H. Cartmell, S.M. Richardson, L.A. Bosworth, Material Characterization of PCL:PLLA Electrospun Fibers Following Six Months Degradation In Vitro., Polymers. 12 (2020). https://doi.org/10.3390/polym12030700.

[22] C.R. Wittmer, A. Hébraud, S. Nedjari, G. Schlatter, Well-organized 3D nanofibrous composite constructs using cooperative effects between electrospinning and electrospraying, Polymer. 55 (2014) 5781–5787. https://doi.org/10.1016/j.polymer.2014.08.044.

[23] S. Nedjari, S. Eap, A. Hébraud, C.R. Wittmer, N. Benkirane-Jessel, G. Schlatter, Electrospun Honeycomb as Nests for Controlled Osteoblast Spatial Organization, Macromol. Biosci. 14 (2014) 1580–1589. https://doi.org/10.1002/mabi.201400226.

[24] A. Harrane, A. Leroy, H. Nouailhas, X. Garric, J. Coudane, B. Nottelet, PLA-based biodegradable and tunable soft elastomers for biomedical applications, Biomed. Mater. 6 (2011) 065006. https://doi.org/10.1088/1748-6041/6/6/065006.

[25] A. Leroy, C. Pinese, C. Bony, X. Garric, D. Noël, B. Nottelet, J. Coudane, Investigation on the properties of linear PLA-poloxamer and star PLA-poloxamine copolymers for temporary biomedical applications, Mater. Sci. Eng. C. 33 (2013) 4133–4139. https://doi.org/10.1016/j.msec.2013.06.001.

[26] L. Gangolphe, S. Déjean, A. Bethry, S. Hunger, C. Pinese, X. Garric, F. Bossard, B. Nottelet, Degradable multi(aryl azide) star copolymer as universal photo-crosslinker for

elastomeric scaffolds, Mater. Today Chem. 12 (2019) 209–221. https://doi.org/10.1016/j.mtchem.2018.12.008.

[27] A. Leroy, A. Al Samad, X. Garric, S. Hunger, D. Noël, J. Coudane, B. Nottelet, Biodegradable networks for soft tissue engineering by thiol–yne photo cross-linking of multifunctional polyesters, RSC Adv. 4 (2014) 32017–32023. https://doi.org/10.1039/C4RA03665D.

[28] L.C. Lins, F. Wianny, S. Livi, I.A. Hidalgo, C. Dehay, J. Duchet-Rumeau, J.-F. Gérard, Development of Bioresorbable Hydrophilic–Hydrophobic Electrospun Scaffolds for Neural Tissue Engineering, Biomacromolecules. 17 (2016) 3172–3187. https://doi.org/10.1021/acs.biomac.6b00820.

[29] T. Yamaoka, Y. Tabata, Y. Ikada, Distribution and Tissue Uptake of Poly(ethylene glycol) with Different Molecular Weights after Intravenous Administration to Mice, J. Pharm. Sci. 83 (1994) 601–606. https://doi.org/10.1002/jps.2600830432.

[30] A. Kowalski, A. Duda, S. Penczek, Polymerization of L , L -Lactide Initiated by Aluminum Isopropoxide Trimer or Tetramer, Macromolecules. 31 (1998) 2114–2122. https://doi.org/10.1021/ma971737k.

[31] J. Coudane, E. Laurent, M. Vert, Poly(?-caprolactone)-Based Organogels and Hydrogels with Poly(ethylene glycol) Cross-Linkings, Macromol. Rapid Commun. 25 (2004) 1865–1869. https://doi.org/10.1002/marc.200400310.

[32] M. Kessler, J. Groll, J. Tessmar, Application of Linear and Branched Poly(Ethylene Glycol)-Poly(Lactide) Block Copolymers for the Preparation of Films and Solution Electrospun Meshes, Macromol. Biosci. 16 (2016) 441–450. https://doi.org/10.1002/mabi.201500238.

[33] H. Mondésert, F. Bossard, D. Favier, Anisotropic electrospun honeycomb polycaprolactone scaffolds: Elaboration, morphological and mechanical properties, J. Mech. Behav. Biomed. Mater. 113 (2021) 104124. https://doi.org/10.1016/j.jmbbm.2020.104124.

[34] Naoshi Hirai, Hiroto Ishikawa, Yoshimichi Ohki, Electrical conduction properties of several biodegradable polymers, in: 2007 Annu. Rep. - Conf. Electr. Insul. Dielectr. Phenom., 2007: pp. 592–595. https://doi.org/10.1109/CEIDP.2007.4451542.

[35] D. Li, Y. Wang, Y. Xia, Electrospinning of Polymeric and Ceramic Nanofibers as Uniaxially Aligned Arrays, Nano Lett. 3 (2003) 1167–1171. https://doi.org/10.1021/nl0344256.

[36] J.L. Lowery, N. Datta, G.C. Rutledge, Effect of fiber diameter, pore size and seeding method on growth of human dermal fibroblasts in electrospun poly(ε-caprolactone) fibrous mats, Biomaterials. 31 (2010) 491–504. https://doi.org/10.1016/j.biomaterials.2009.09.072.

[37] C. Del Gaudio, A. Bianco, M. Folin, S. Baiguera, M. Grigioni, Structural characterization and cell response evaluation of electrospun PCL membranes: Micrometric versus submicrometric fibers, J. Biomed. Mater. Res. A. 89A (2009) 1028–1039. https://doi.org/10.1002/jbm.a.32048.

[38] C. Vaquette, J.J. Cooper-White, Increasing electrospun scaffold pore size with tailored collectors for improved cell penetration, Acta Biomater. 7 (2011) 2544–2557. https://doi.org/10.1016/j.actbio.2011.02.036.

[39] Q.L. Loh, C. Choong, Three-dimensional scaffolds for tissue engineering applications: role of porosity and pore size, Tissue Eng. Part B Rev. 19 (2013) 485–502. https://doi.org/10.1089/ten.TEB.2012.0437.

[40] W. Cui, X. Zhu, Y. Yang, X. Li, Y. Jin, Evaluation of electrospun fibrous scaffolds of poly(dl-lactide) and poly(ethylene glycol) for skin tissue engineering, Mater. Sci. Eng. C. 29 (2009) 1869–1876. https://doi.org/10.1016/j.msec.2009.02.013.

[41] W. Wang, G. Caetano, W.S. Ambler, J.J. Blaker, M.A. Frade, P. Mandal, C. Diver, P. Bártolo, Enhancing the Hydrophilicity and Cell Attachment of 3D Printed PCL/Graphene Scaffolds for Bone Tissue Engineering, Mater. Basel Switz. 9 (2016) 992. https://doi.org/10.3390/ma9120992.

[42] M.R. Alexander, P. Williams, Water contact angle is not a good predictor of biological responses to materials, Biointerphases. 12 (2017) 02C201. https://doi.org/10.1116/1.4989843.

[43] C.Y. Leon-Valdivieso, A. Garcia-Garcia, C. Legallais, F. Bedoui, Electrospinning of biomedically relevant multi-region scaffolds: From honeycomb to randomly-oriented microstructure, Polymer. 202 (2020) 122606. https://doi.org/10.1016/j.polymer.2020.122606.

[44] Y.K. Choi, Y.H. Bae, S.W. Kim, Star-Shaped Poly(ether–ester) Block Copolymers: Synthesis, Characterization, and Their Physical Properties, Macromolecules. 31 (1998) 8766–8774. https://doi.org/10.1021/ma981069i.

[45] C.F. Guimarães, L. Gasperini, A.P. Marques, R.L. Reis, The stiffness of living tissues and its implications for tissue engineering, Nat. Rev. Mater. 5 (2020) 351–370. https://doi.org/10.1038/s41578-019-0169-1.

[46] D.F. Williams, Challenges With the Development of Biomaterials for Sustainable Tissue Engineering, Front. Bioeng. Biotechnol. 7 (2019) 127. https://doi.org/10.3389/fbioe.2019.00127.

[47] D.S.-G. Hu, H.-J. Liu, Structural analysis and degradation behavior in polyethylene glycol/poly(L-lactide) copolymers, J. Appl. Polym. Sci. 51 (1994) 473–482. https://doi.org/10.1002/app.1994.070510310.

[48] M. Vert, Degradable and bioresorbable polymers in surgery and in pharmacology: beliefs and facts, J. Mater. Sci. Mater. Med. 20 (2009) 437–446. https://doi.org/10.1007/s10856-008-3581-4.

[49] M. Hakkarainen, A.-C. Albertsson, S. Karlsson, Weight losses and molecular weight changes correlated with the evolution of hydroxyacids in simulated in vivo degradation of homo- and copolymers of PLA and PGA, Polym. Degrad. Stab. 52 (1996) 283–291. https://doi.org/10.1016/0141-3910(96)00009-2.

[50] D.D. Lu, J.C. Yuan, H. Li, Z.-Q. Lei, Synthesis and characterization of a series of biodegradable and biocompatible PEG-supported poly(lactic-ran-glycolic acid) amphiphilic barbell-like copolymers, J. Polym. Sci. Part Polym. Chem. 46 (2008) 3802–3812. https://doi.org/10.1002/pola.22729.

[51] T. Kissel, Y. Li, F. Unger, ABA-triblock copolymers from biodegradable polyester A-blocks and hydrophilic poly(ethylene oxide) B-blocks as a candidate for in situ forming hydrogel delivery systems for proteins, Adv. Drug Deliv. Rev. 54 (2002) 99–134. https://doi.org/10.1016/S0169-409X(01)00244-7.

[52] E. Girard, G. Chagnon, A. Moreau-Gaudry, C. Letoublon, D. Favier, S. Dejean, B. Trilling, B. Nottelet, Evaluation of a biodegradable PLA–PEG–PLA internal biliary stent for liver transplantation: in vitro degradation and mechanical properties, J. Biomed. Mater. Res. B Appl. Biomater. 109 (2021) 410–419. https://doi.org/10.1002/jbm.b.34709.

[53] Y. Fukuhira, E. Kitazono, T. Hayashi, H. Kaneko, M. Tanaka, M. Shimomura, Y. Sumi, Biodegradable honeycomb-patterned film composed of poly(lactic acid) and dioleoylphosphatidylethanolamine, Biomaterials. 27 (2006) 1797–1802. https://doi.org/10.1016/j.biomaterials.2005.10.019.

[54] S. Nedjari, F. Awaja, G. Altankov, Three Dimensional Honeycomb Patterned Fibrinogen Based Nanofibers Induce Substantial Osteogenic Response of Mesenchymal Stem Cells, Sci. Rep. 7 (2017). https://doi.org/10.1038/s41598-017-15956-8.

[55] X. Zhu, W. Cui, X. Li, Y. Jin, Electrospun Fibrous Mats with High Porosity as Potential Scaffolds for Skin Tissue Engineering, Biomacromolecules. 9 (2008) 1795–1801. https://doi.org/10.1021/bm800476u.

[56] J.M. Ameer, A.K. PR, N. Kasoju, Strategies to Tune Electrospun Scaffold Porosity for Effective Cell Response in Tissue Engineering, J. Funct. Biomater. 10 (2019). https://doi.org/10.3390/jfb10030030.

[57] C. Ru, F. Wang, M. Pang, L. Sun, R. Chen, Y. Sun, Suspended, Shrinkage-Free, Electrospun PLGA Nanofibrous Scaffold for Skin Tissue Engineering, ACS Appl. Mater. Interfaces. 7 (2015) 10872–10877. https://doi.org/10.1021/acsami.5b01953.